Enhanced Heat Transfer, 1999, Vol. 6, pp. 343–355
Reprints available directly from the publisher
Photocopying permitted by license only

Enhancement of R123 Pool Boiling by the Addition of *N*-hexane

M. A. KEDZIERSKI*

National Institute of Standards and Technology, Bldg. 226, Rm B114, Gaithersburg, MD 20899

(Received in final form 20 May 1998)

This paper presents the heat transfer data used to file international patent WO 94/18282. The data consisted of pool boiling performance of a GEWA-T^{TM} surface for three fluids: (1) pure R123, (2) R123/*n*-hexane (99/1), and (3) R123/*n*-hexane (98/2). The heat flux and the wall superheat were measured for each fluid at 277.6 K. A (47 ± 7)% increase over the pure R123 heat flux was achieved with the addition of 1% mass hexane to R123. Similarly, the R123/hexane (98/2) mixture gave a maximum percent heat flux enhancement over pure R123 of (29 ± 7)%. The boiling was filmed with a 16 mm high-speed camera. The observations were used to describe various boiling modes on the GEWA-T^{TM} surface. The addition of hexane to pure R123 caused a simultaneous reduction in the bubble diameter and increase in the site density. The increase in site density enhanced the boiling despite the reduction in bubble size. Presumably, the site density enhancement was caused by a layer enriched in hexane at the heat transfer surface.

Keywords: Enhanced heat transfer, additive, R123, pool boiling, GEWA-T^{TM}, fluid heating, *n*-hexane, surfactant

INTRODUCTION

Typically, binary mixtures exhibit a boiling performance degradation compared to their pure components (Shock, 1982 and Thome, 1990). Yet, some special liquids, when added in small quantities, enhance the boiling performance of pure fluids. For the refrigeration and air-conditioning industry, a liquid additive would be an economical means of reducing manufacturing and/or operating costs. For example, a liquid additive for 1,1-dichloro-2,2,2-trifluoroethane (R123) would enable existing water chillers to operate more efficiently or enable new water chillers to meet the same duty with less tubes. Unfortunately, liquid additives that significantly enhance refrigerant boiling performance are rare.

Most of the work on liquid additives has been in surfactants for aqueous solutions (Jontz and Myers (1960), Shah and Darby (1973) and Wu

* Corresponding author. Tel: 301-975-5282, Fax: 301-975-4032.

et al. (1995)). Carey (1992) and Rosen (1978) describe how surfactants reduce the surface-tension of water. Basically, the surfactant molecule must have polar and nonpolar ends, *i.e.*, an amphipathic structure. The nonpolar end of the surfactant distorts the interior structure of the solution. The structural distortion requires less work to bring a surfactant molecule to the liquid–vapor interface than is required to bring a water molecule to the surface. By definition, the surface-tension of the liquid–vapor interface is lowered when less work is required to bring a molecule to the surface.

Not much research has been done in surfactants for refrigerants. Aqueous surfactant solutions are relatively common because the surface-tension of water is greater than that of many liquids with amphipathic structures. Typically, the surface-tension of refrigerants is lower than that of amphipathic liquids. Consequently, it is difficult to find a surfactant to lower the liquid–vapor surface-tension of a refrigerant.

APPARATUS

Figure 1 shows a schematic of the apparatus used to measure the pool boiling data of this study. The apparatus was used to measure the liquid saturation temperature (T_s), the average pool-boiling heat flux (q''), and the wall temperature (T_w). The three principal components of the apparatus were: test chamber, condenser, and reservoir. The internal dimensions of the test chamber were 25.4 mm × 257 mm × 1.54 m. The test chamber was charged with approximately 7 kg of R123 from the reservoir, giving a liquid height of approximately 80 mm above the test surface. The bottom of the test section, as shown in Figure 1, was heated with high velocity (2.5 m/s) water flow. The vapor produced by liquid boiling on the test surface was condensed by the brine-cooled, shell-and-tube condenser and returned as liquid to the pool by gravity.

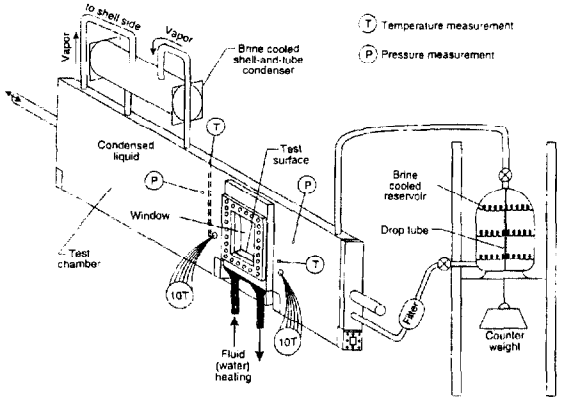

FIGURE 1 Schematic of test apparatus.

As shown in Figure 1, the test section was visible through two opposing, flat 150 × 200 mm quartz windows. A high-speed camera was used to film the boiling at 1000, 3000, and 6000 frames per second (fps). Two 500 W forward lights illuminated the specimens during filming. Films were taken at selected heat fluxes immediately after the measurement of the heat-transfer coefficient to ensure that the heat from the lights did not influence the measurement.

Several precautions were taken to reduce the errors associated with the liquid saturation temperature measurement. The saturation temperature of the liquid was measured with a 450 mm long 1.6 mm diameter stainless steel sheathed thermocouple. The small diameter provided for a relatively rapid response time. Nearly the entire length of the thermocouple was in contact with either the test refrigerant vapor or liquid to minimize conduction errors. The tip of the thermocouple was placed approximately 2 mm above and 200 mm to the left of the top of the test surface. This placement ensured that approximately 80 mm of the probe length was in relatively well-mixed liquid near the two-phase fluid above the test surface. To provide for a saturated liquid pool state, the mass of liquid in the pool was large compared to mass of liquid condensed. At the highest heat flux, it would require nearly one hour to evaporate and condense the entire test chamber charge. Convection and radiation errors were

minimal due to low (277.6 K), uniform temperatures attributed to well-insulated, low emissivity, 38 mm aluminum test chamber walls.

MEASUREMENTS AND UNCERTAINTIES

The standard uncertainty (u_i) is the positive square root of the estimated variance u_i^2. The individual standard uncertainties are combined to obtain the expanded uncertainty (U). The expanded uncertainty is commonly referred to as the law of propagation of uncertainty with a coverage factor. All measurement uncertainties are reported for a 95% confidence interval.

The copper-constantan thermocouples were calibrated against a standard in the NIST Temperature Group to a residual standard deviation of 0.005 K. Considering the fluctuations in the saturation temperature during the test and the standard uncertainties in the calibration, the expanded uncertainty of the average saturation temperature was no greater than 0.04 K. A thermocouple drift of within 0.1 K was determined by recalibrating the thermocouples one year after the tests were completed. Consequently, the expanded uncertainty of the temperature measurements was less than 0.1 K. The saturation temperature was also obtained from a pressure transducer measurement with an uncertainty of less than 0.03 kPa. The uncertainty of the saturation temperature from equilibrium data (Morrison and Ward, 1991) for R123 was 0.17 K. Vapor–liquid equilibrium data for the R123/hexane mixtures were obtained from Shealy (1993). An equation of state (Morrison and McLinden, 1985) was used to extend the mixture equilibrium data to the operating conditions and mixture compositions of the test. The saturation temperature obtained from the thermocouple and the pressure measurement always agreed within ± 0.17 K.

Figure 2 shows the coordinate system for the 20 wells where the thermocouples where force fitted into the side of the test plate. The wells were 16 mm deep to reduce conduction errors. Using a

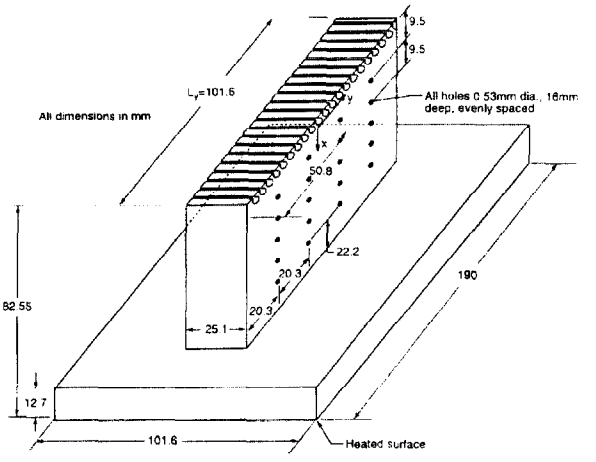

FIGURE 2 OFHC copper GEWA-T^{TM} test plate and thermocouple coordinate system.

method given by Eckert and Goldstein (1976), errors due to heat conduction along the thermocouple leads were estimated to be well below 0.01 mK. The origin of the coordinate system was centered on the surface with respect to the y-direction at the root of the fin. Centering the origin in the y-direction improved the accuracy of the wall heat flux and temperature calculations by reducing the number of fitted constants involved in these calculations. The x-coordinate measures the distance normal to the heat transfer surface. The y-coordinate measures the distance perpendicular to the x-coordinate. The thermocouples were arranged in four sets of five aligned in the x-direction. Following a procedure given by Kedzierski and Worthington (1993), the size and arrangement of the thermocouple wells were designed to minimize the errors in the wall temperature and temperature gradient measurement.

The heat flux and the wall temperature were obtained by regressing the measured temperature distribution of the block to the governing conduction equation. In other words, rather than using the boundary conditions to solve for the interior temperatures, the interior temperatures were used to solve for the boundary conditions following a procedure given in Kedzierski (1995). Two solutions

were found: one for pure R123 for heat fluxes below 10 kW/m^2:

$$T = A_0 + A_1 x + A_2 y \tag{1}$$

and another for R123/hexane mixtures and pure R123 heat fluxes above 10 kW/m^2:

$$T = A_0 + A_1 x + A_2 y + A_3(x^2 - y^2) + A_4 y(3x^2 - y^2) \tag{2}$$

Fourier's law and the fitted constants (A_0, A_1 and A_3) were used to calculate the average wall heat flux (q'') normal to the heat transfer surface for both the first and third order models as:

$$q'' = \left(\frac{1}{L_y} \int_{-L_y/2}^{L_y/2} k \frac{\partial T}{\partial x} dy \right)_{x=0} = \bar{k} A_1 \tag{3}$$

where $\bar{k}$ is the average thermal conductivity along the surface of the plate, and L_y is the length of the heat transfer surface as shown in Figure 2.

The average wall temperature for the first order model is:

$$\overline{T_w} = \left(\frac{1}{L_y} \int_{-L_y/2}^{L_y/2} T dy \right)_{x=0} = A_0 \tag{4}$$

and that for the third order model is:

$$\overline{T_w} = A_0 - \frac{A_3 L_y^2}{12} \tag{5}$$

A particular model was chosen if it produced the smallest uncertainties in the heat flux and wall temperature calculations. In addition, the model must maintain nearly the same residual standard deviation as the model containing the first nine terms of the two-dimensional Laplace equation. For approximately half of the mixture data, the A_2 constant was set to zero to obtain smaller uncertainties in q'' and T_w.

Siu *et al.* (1976) estimated the uncertainty in the thermal conductivity of OFHC copper to be about 2 to 3% by comparing round-robin experiments. Considering this, the relative expanded uncertainty in q'' was greatest at the lowest heat fluxes, approaching 10% of the measurement at 10 kw/m^2. In general, the $E_{q''}$ appears to be relatively constant between 6% and 3% for heat fluxes above 30,000 W/m^2. The average random error in the wall superheat – $\Delta T_s = \overline{T_w} - T_s$ – was within 0.1 K. A more detailed discussion of the uncertainty analysis can be found in Kedzierski (1996).

TEST SURFACE

Figure 2 shows the oxygen-free high-conductivity (OFHC) copper GEWA-T^{TM} test plate used in this study. Commercially, the GEWA-T^{TM} or "*T*-fin" surface is formed by flattening the tips of the GEWA-K^{TM} surface. The GEWA-T^{TM} surface in this study was machined directly onto the top of the test plate by electric discharge machining (EDM). Figure 3 shows a photograph of the fin surface. The gap between the fin-tips was 0.348 mm. The surface had approximately 667 fins per meter oriented along the short axis of the plate. The ratio of the surface area to the projected area of the surface was 2.47. The fin-tip width and the fin-height were 1.05 mm and 1.038 mm, respectively.

Gewa-T Pool-boiling

The heat flux was varied from 10 kw/m^2 to 80 kW/m^2 to simulate typical operating conditions of R123 chillers equipped with enhanced tubes. All evaporation tests were taken at 277.6 K. The data were recorded consecutively starting at approximately 74 kW/m^2, increasing up to 80 kW/m^2, and

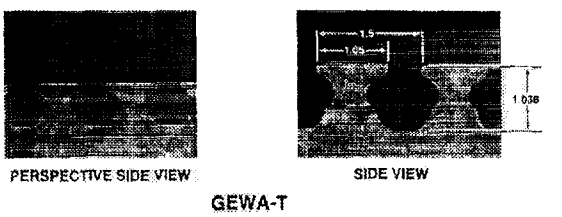

FIGURE 3 Photograph of GEWA-T^{TM} geometry.

then descending to $20\,kW/m^2$ in intervals of approximately $4\,kW/m^2$. The descending heat flux procedure minimized the possibility of any hysteresis effects on the data which would have made the data sensitive to the initial operating conditions.

The mixtures were prepared by charging measured weights of R123 and spectrophotometric grade hexane into an evacuated reservoir (see Fig. 1). All compositions are given on a mass percent basis. The liquid was injected into a drop tube that nearly touched the bottom of the reservoir. First, approximately 90% of the R123 was charged. Then the hexane was injected with a syringe through the drop tube, followed by flushing with the remaining R123 charge. The flushing of R123 through the drop tube also assisted in mixing the sample. The amount of R123 that remained in the drop tube after flushing had a negligible effect on the composition. The heat-transfer test chamber was charged with the test fluid from this reservoir.

Three compositions were investigated: (1) pure R123, (2) R123/hexane (99/1), and (3) R123/hexane (98/2). Figures 4 through 6 are plots of the measured heat flux (q'') *versus* the measured wall superheat ($T_w - T_s$). The pure R123, the R123/hexane (99/1), and the R123/hexane (98/2) data were taken over four, five and two days, respectively. One complete run was done in a single day. The solid line is a best-fit regression or

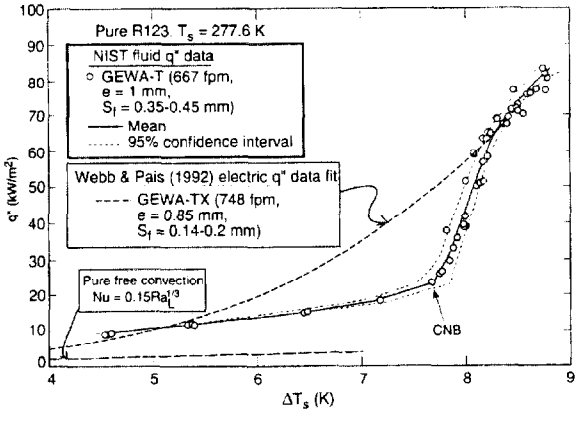

FIGURE 4 Boiling curve for pure R123 at 277.6 K on the GEWA-T surface.

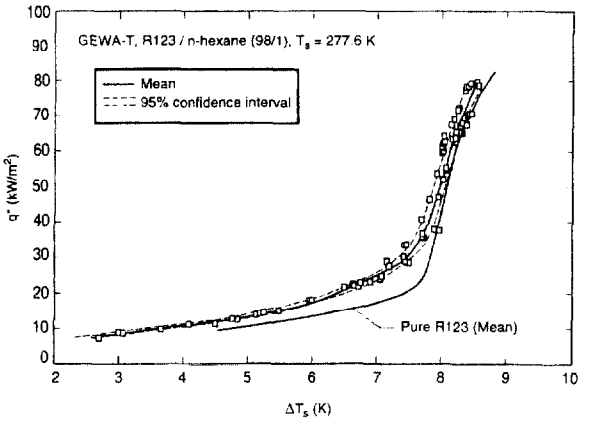

FIGURE 5 Comparison of the R123/hexane (99/1) boiling data to the mean of the R123 data.

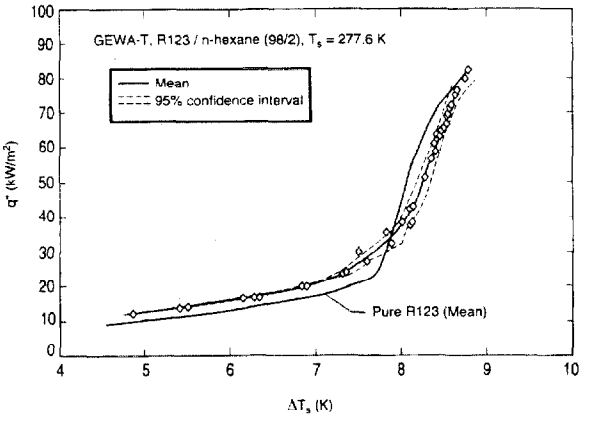

FIGURE 6 Comparison of the R123/hexane (98/2) boiling data to the mean of the R123 data.

estimated mean of the data. The dashed lines to either side of the mean represent the lower and upper 95% simultaneous (multiple-use) confidence intervals for the mean. The expanded uncertainty of the estimated mean wall superheat in the natural convection region and the boiling region is approximately 0.1 K and 0.07 K, respectively. The figures illustrate that, depending upon the operating condition and composition, R123/hexane mixtures exhibited a heat transfer enhancement compared to pure R123.

Figure 4 presents the boiling curve for pure R123 at 277.6 K on the GEWA-T surface. The

boiling curve exhibits two characteristic regimes: a natural convection regime and a nucleate boiling regime.

The regimes are separated by the cessation of nucleate boiling (CNB). A well-defined CNB occurs for the pure R123 data at approximately 7.6 K (20.2 kW/m^2). The nucleate boiling regime exists for superheats greater than the CNB condition. Here, the heat transfer is governed primarily by the formation of isolated bubbles within the fin cavities. The superheats below the CNB are insufficient to support vigorous bubble generation. Consequently, natural convection becomes a prevalent mode of heat transfer for superheats below CNB. In this region, only severely limited bubble activity exists. However, it is possible that microscopic bubbles were produced in the natural convection region that were not visible in the high-speed films.

Figure 4 also compares the present GEWA-T^{TM} boiling curve to GEWA-TX^{TM} boiling curve measured by Webb and Pais (1992) at equal saturation temperatures. The figure summarizes the geometry differences between the plate tested in this study and the tube that Webb and Pais (1992) tested. The Webb and Pais (1992) GEWA-TX^{TM} data agree with the present data for heat fluxes above 50 kW/m^2 and below 10 kW/m^2 and is greater than the present data for intermediate heat fluxes. The maximum percent difference of 100% occurs at CNB.

The greater performance of the Webb and Pais (1992) GEWA-TX^{TM} surface in the intermediate heat flux region was partly due to the greater fpm and the additional notch enhancement of the GEWA-TX^{TM} surface. Also, the gap between the fins (S_f) on the plate was significantly larger than that on the GEWA-TX^{TM} tube. The smaller fin-gap and the notch are effective at enhancing heat transfer at low site densities. A narrower fin-gap encourages bubble coalescence within the cavity. The notch acts to increase the site density. As the site density increases with the heat flux and the surface becomes saturated with bubbles, these geometry effects becomes less effective at heat transfer enhancement. Also, as reported by Cornwell and Einarsson (1989), a flat plate does not experience the convection that is induced by bubbles that slide within the channels of the side of a tube. The sliding bubbles also act to seed upper portions of the tube with vapor. These mechanisms would be less influential at higher heat fluxes where most of the potential sites have become active with vigorous bubble activity. Consequently, the performance difference between the plate and the tube becomes less significant at larger heat fluxes.

Figure 4 also shows the predictions from a free convection correlation for a horizontal plate with the upper surface being heated which was recommended by Incropera and Dewitt (1985). Although, the correlation is for a flat plate, it may be possible to account for the enhanced surface with the characteristic length defined as the surface area over the exterior perimeter of the plate. The predictions are substantially lower than the present measurements. The free convection on the test surface may have been enhanced by the upward motion of bubbles that were unavoidably generated near its exterior perimeter. In addition, an occasional site would be active on the surface which may have also contributed to the enhanced free convection.

Figure 5 compares the R123/hexane (99/1) boiling data to the mean of the R123 data. The addition of 1% mass hexane to R123 has improved the boiling performance in two ways: (1) the average R123/hexane (99/1) mixture heat flux is approximately 24% above that of pure R123 for heat fluxes from 8 kW/m^2 to 73 kW/m^2, and (2) the 99/1 mixture boils at superheats smaller than the CNB of pure R123. Lower superheats required for boiling permit evaporators to operate at lower approach temperature differences which leads to more efficient operation of refrigeration equipment. Higher heat fluxes could be used to either reduce the required size of the evaporator or to improve the efficiency of existing refrigeration equipment.

Figure 6 shows that a doubling of the hexane concentration results in an average heat flux

.tion of 5% over the range of 10 kW/m^2 to n^2. Essentially, only natural convection w heat flux boiling heat transfer are ed. A heat transfer degradation occurs at ixes above 34 kW/m^2. The CNB for both 1 and the 98/2 mixtures is not as clearly as it is for pure R123. The gradual on from the boiling to natural convection s that boiling does not cease as abruptly for xture as it does for the pure R123. ntly, more sites are active for the mixture at lower heat fluxes as compared to the 123.

re 7 summarizes the effect of the addition of to R123 on the R123 heat flux. The figure ie ratio of the mixture to the pure R123 heat $r''_{1\%}/q''_p$ or $q''_{2\%}/q''_p$) *versus* the pure R123 ux (q''_p) at the same wall superheat. A heat r enhancement exists where the heat flux is greater than one and the confidence ls do not include the value one. Accordthe R123/hexane (99/1) mixture exhibits an ement for entire heat flux range that was while the R123/hexane (98/2) mixture s an enhancement for heat fluxes below imately 30 kW/m^2.

ice that the heat flux ratios for the two es have similar forms suggesting that a of curves may exist for various composi-Both exhibit a maximum at a R123 heat flux of approximately 23 kW/m^2. The maximum is probably a result of the cessation of boiling for pure R123 while the mixture boiling continues at 23 kW/m^2. At this point, the maximum percent heat flux enhancement is (47 ± 7)% for the 99/1 mixture and (29 ± 7)% for the 98/2 mixture. An average enhancement of 19% exists from 10 kW/m^2 to 33.5 kW/m^2 for the 98/2 mixture. The average enhancement is consistent with a 13% to 20% increase in the evaporation heat transfer coefficient with the addition of 1% mass *n*-Pentane to R123 which was measured by the Trane Company (Glamm, 1995). The mean enhancement for the 99/1 mixture never dropped below 5% for all test conditions. By contrast, the 98/2 mixture exhibited an average degradation of 18% within the range of 33.5 kW/m^2 to 80 kW/m^2.

Figure 7 also provides 95% simultaneous confidence intervals for the enhancement ratios for the 99/1 and 98/2 mixtures. Because the confidence intervals for the 99/1 mixture are both greater than unity, an enhancement exists for all of the heat fluxes tested for 95% confidence. Figure 7 shows that a degradation exists for the 98/2 mixture for heat fluxes above 45 kW/m^2.

VISUAL OBSERVATIONS

Figures 8 through 13 show sketches of the bubble activity of the Gewa-T surface which were taken from 16 mm high-speed film. The quartz window

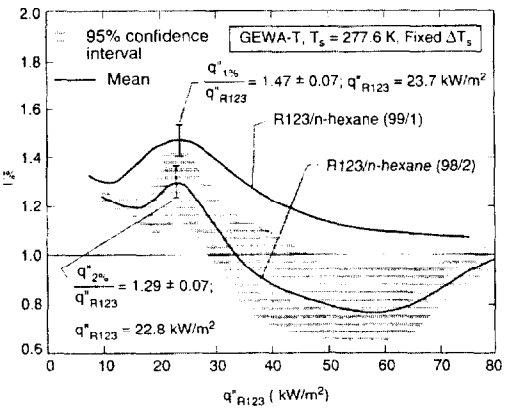

RE 7 Effect of hexane on R123 pool boiling heat flux.

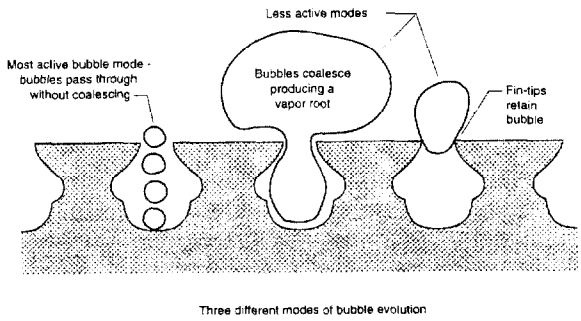

FIGURE 8 Three boiling modes for R123 at 70 kW/m^2.

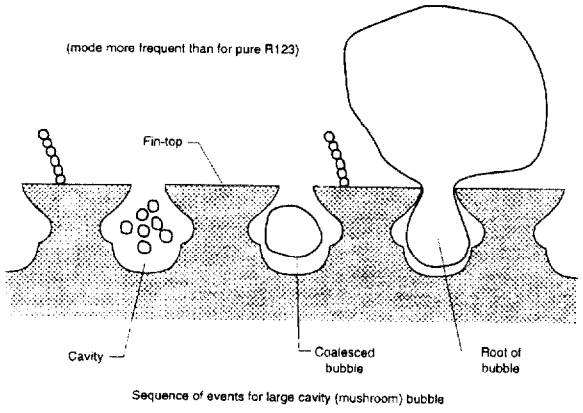

FIGURE 9 Mushroom bubble mode for R123/hexane (99/1) at 70 kW/m^2.

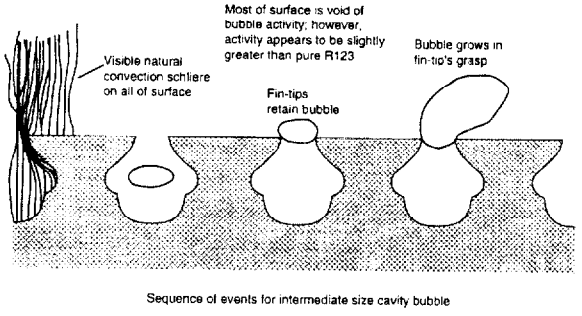

FIGURE 10 Intermediate bubble mode for R123/hexane (99/1) at 30 kW/m^2.

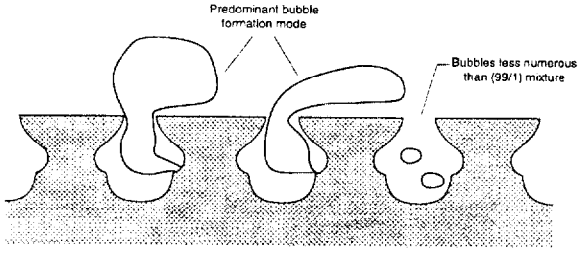

FIGURE 11 Bubble activity for R123/hexane (98/2) at 70 kW/m^2.

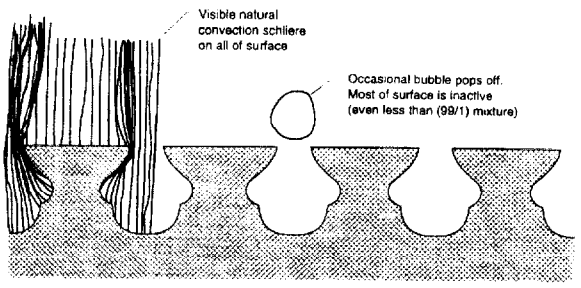

FIGURE 12 Bubble activity for R123 at 30 kW/m^2.

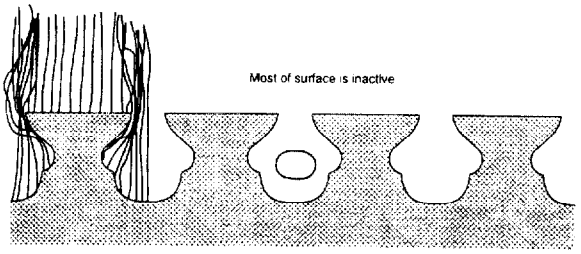

FIGURE 13 Bubble activity for R123/hexane (99/2) at 30 kW/m^2.

covered the sides of the plate so that the bubble activity within the cavities was visible while looking down the channels. These figures are schematics of the bubble activity for the three test fluids at two different heat fluxes. A comparison of the figures illustrates that the enhancement mechanism is similar to that caused by lubricants as described in Kedzierski (1993) and Kedzierski and Kaul (1993). The addition of hexane to pure R123 causes a simultaneous reduction in the bubble diameter and increase in the site density. Tzan and Yang (1990) also observed this same trend for surfactants in aqueous solutions.

Figure 8 depicts the three different boiling modes for R123 at $q'' = 70\,\text{kW/m}^2$. Each mode depends on the size of the bubble as it exists when it is in the cavity. The bubble modes for small, large (mushroom), and intermediate size bubbles are illustrated from left to right in Figure 8. The small cavity-bubble formation mode occurs when small diameter bubbles (0.26 mm to 0.32 mm) are individually formed and travel unobstructed through the gap between the fins. The small bubble formation mode dominated approximately 70% of the bubble formation occurrences.

Figure 9 depicts the sequence of events that describe the large cavity-bubble mode. First, several small bubbles are almost simultaneously

formed. If the bubbles are sufficiently congested within the cavity, they will coalesce into one large bubble. Due to the close proximity of the bubble to the cavity walls, the bubble receives energy from the superheated liquid and ejects vapor through the fin gap, while maintaining a vapor root within the cavity. When the buoyancy force on the portion of the bubble above the fins is large enough, it will cause the vapor root to be pulled out of the cavity.

Figure 10 illustrates the bubble formation mode for intermediate size bubbles. This mode occurs when a cavity bubble is larger than the gap between the fins, but not large enough to get close to the superheated liquid layer to grow rapidly. The bubble is retained by the fin tips. It receives energy directly from the corners of the fin and grows until buoyancy forces pull the bubble from the fin. The last two boiling modes are advantageous since they efficiently create additional vapor. That is, vapor is generated at a lower superheat for a large bubble while much of its surface area is in contact with the superheated liquid of the cavity. The intermediate and large cavity-bubble modes occurred at about equal frequencies and together contributed to 30% of the bubble activity.

The above visual observations contradict the mechanistic model of Ayub and Bergles (1987) for pool boiling of water and R113 from GEWA surfaces. The Ayub and Bergles (1987) model assumes that a large vapor seed fills the channel with the exception of a thin liquid film that lies between the vapor and the cavity wall. Their model assumes that the vapor–liquid interface of the bubble is in contact with the gaps between the tops of the fins. The liquid–vapor interface drops below the tops of the fins at inactive areas along the fin gap to permit the thin liquid film to be replenished while the near-cavity-size vapor seed remains in the cavity. This contradicts the present mechanistic description where the cavity is filled primarily with liquid and the bubbles originate from micro-vapor seeds at the cavity root.

Figure 9 depicts that the R123/hexane (99/1) mixture exhibited a greater active site density (based on the cavity area) than did the pure R123. The cavity bubbles were smaller, but more numerous. Also, 0.1 mm diameter bubbles generated on the tops of the fins were visible for the R123/hexane (99/1) mixture, but were not visible for pure R123 nor the 98/2 mixture. Apparently, the addition of hexane caused an increase in the active site density.

In general, the R123/hexane (99/1) mixture exhibited more smaller diameter bubbles (0.2 mm) than pure R123 exhibited. Consequently, because a greater number of small bubbles increases the probability of coalescence within the cavity, the 99/1 mixture also exhibited more mushroom cavity-bubbles. The bubble activity was approximately split between the mushroom and the small bubble modes while the intermediate bubble mode appeared to be absent for the 99/1 mixture. It is likely that the heat transfer was enhanced for the 99/1 mixture by the production of more small and mushroom bubbles.

Figure 11 depicts that the R123/hexane (98/2) mixture had a smaller active site density than that of the 99/1 mixture. As compared to the 99/1 mixture bubbles, the 98/2 mixture bubbles were marginally smaller (0.18 mm on average) and were less numerous. As a result, the heat transfer performance of the 98/2 mixture is less than that of the 99/1 mixture. Also, no 98/2 mixture bubbles were generated on the tops of the fins. The mushroom bubbles dominated the bubble activity; however, instead of originating from coalesced bubbles, the mushroom bubbles grew directly from the side of the cavity wall.

A summary of representative bubble characteristics at 70 kW/m^2 is given below. These are only representative values obtained from averaging the available data. A wide range of bubble frequencies and site density existed for each fluid. The individual frequency for the small bubbles and the mushroom bubbles was nearly the same for the three fluids tested: approximately 340 bubbles/sec and 75 bubbles/sec, respectively. The R123/hexane (99/1) mixture produced approximately 70% more bubbles than the pure R123. Approximate values

for the site density per channel are: 22,000 sites/m^2, and 13,000 sites/m^2 for the R123/hexane (99/1) and the pure R123, respectively. The site density of R123/hexane (99/2) was approximately 17,000 sites/m^2.

Figures 10, 12 and 13 are schematics of the bubble activity for the three test fluids at $q'' = 30\,\text{kW/m}^2$. Natural convection density gradients or Schliere were visible over the entire surface for all test fluids. Most of the heat transfer surface was inactive with the exception of a few sparse sites. Mushroom bubbles were not present. The R123/hexane (99/1) appeared to have the most bubble activity of the fluids at 30 kW/m^2. R123 and the 98/2 mixture had similar but lower bubble activities at 30 kW/m^2.

ENHANCEMENT MECHANISM SPECULATION

The visual observations have shown that the R123/hexane (99/1) bubbles are smaller and more numerous than those for pure R123. It is reasonable to assume that the boiling heat transfer is enhanced by the increase in the number of bubbles produced despite the reduction in their size. In other words, a favorable balance between an increase in site density and a reduction in bubble size results in a heat transfer enhancement. Conversely, a heat transfer degradation from loss of bubble size may result despite a corresponding site density increase. An overall description of the boiling mechanism is given below. Then an explanation is offered for why the mixture bubbles are smaller and more numerous than the pure R123 bubbles.

It is speculated that the pool boiling enhancement mechanism associated with the addition of hexane to R123 is due to an accumulation of hexane at the boiling surface. The excess concentration arises from the relatively low vapor pressure of hexane when compared to R123. The hexane can be drawn out of solution as a consequence of refrigerant evaporation. The R123/hexane liquid mixture travels to the heated wall, and the R123 preferentially evaporates from the surface leaving behind a liquid phase enriched in hexane. A balance between deposition and removal of the hexane establishes some unknown excess concentration of hexane at the surface. Effectively, two soluble solutions of R123 and hexane exist: the dilute solution in the bulk and the hexane-rich solution in a thin layer on the root surface of the channel.

Indirect experimental evidence for a boiling induced excess layer is the improvement of the heat transfer performance with the duration of the test. At the start of each test day the mixture was boiled at the highest heat flux for approximately three hours to allow the heat transfer performance to increase and level off. The initial performance would approximately reproduce the pure R123 value and increase to that reported here. Most of the performance gain was seen within the first hour of testing. Apparently, the hexane-rich layer was established during this "break-in" period.

Boiling Region

Unlike typical surfactants, the surfactant reported here does not lower the surface-tension of the liquid–vapor interface. Rather, the present surfactant lowers the surface-tension of the solid–liquid interface through the existence of a liquid excess layer on the solid. The small attractive forces between the hexane-rich excess layer and the heat transfer surface cause a reduction in the departure diameter of the bubbles. Although less heat transfer occurs with a smaller bubble, the site density can be increased as a direct consequence of the small bubble size. An enhancement of the boiling is achieved if the increase in site density more than compensates for the decrease in bubble size. The next few paragraphs provide a more detailed speculative discussion on the enhancement mechanism for R123/hexane mixture pool boiling.

The R123/hexane bubbles are small due to the existence of the hexane-rich excess layer at the

boiling surface. For a surface excess concentration of the solute (Γ), the Gibbs adsorption equation for a dilute solution (Rosen, 1978) predicts a reduction in the surface-tension or surface energy between the mixture and the solid surface:

$$d\sigma = -RT_i\Gamma d\ln C \tag{6}$$

where R is the universal gas constant, T_i is the temperature of the solid-liquid interface, and C is the molar concentration of the solute. If the concentration of the solute (hexane) is increased above the bulk concentration ($\Gamma \neq 0$), then the surface-tension (σ) between interfacing materials will be lower (negative sign in Gibbs eqn.) than what it would have been if the interface concentration was at the bulk composition. A reduction in the surface-tension between a liquid and a boiling surface will induce a corresponding reduction in the size of the departing bubbles. The surface-tension between the liquid and the solid (σ_{ls}) determines the magnitude of the bubble attachment force by establishing the magnitude of the contact angle (β). This can be demonstrated with the use of the Young and Dupré equation (Adamson, 1967) which is a lateral force balance on a bubble attached to a surface:

$$\beta = \arccos\left(\frac{\sigma_{vs} - \sigma_{ls}}{\sigma_{lv}}\right) \tag{7}$$

For fixed surface tension between the liquid and the vapor (σ_{lv}) and the vapor and the solid (σ_{vs}), a reduction in σ_{ls} causes a reduction in the contact angle β. The bubble is held to the wall by a surface tension force proportional to $\sigma_{lv}\sin\beta$. The size of the bubble determines the buoyancy forces on the bubble acting to detach the bubble. A smaller contact angle induces a smaller bubble attachment force and consequently, a smaller bubble size. Accordingly, the mixture bubbles are smaller than the pure R123 bubbles.

Hsu's (1962) site-activation model can be used to show that smaller bubbles will induce higher site densities than larger bubbles. Figure 14 schematically illustrates the proposed site enhancement

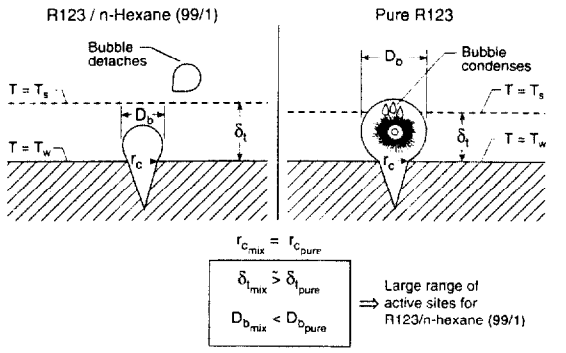

FIGURE 14 Site density enhancement model.

mechanism by comparing the growth of R123/hexane and R123 bubbles in identical conical cavities. Both bubbles originate below the thermal boundary layer thickness (δ_t) which exists as a thin layer near the heated surface where $T > T_s$. According to Hsu's (1962) model, a site will be active if the bubble is released from the wall before it grows beyond the thermal boundary layer. A bubble that grows beyond δ_t while attached to the wall condenses and causes the site to be inactive. For a given cavity distribution, more of the larger cavities will be active for the mixture than for the pure R123.

An increase in the number of active sites is also induced in another way by the smaller bubble size. Westwater (1956) shows that the probability of bubble nucleation increases when less work is required to form a bubble. Less work is required to form small bubbles than large bubbles. The increase in site density for small bubbles is probably due to the coupled effects of lower bubble formation work and the bubble's growth within the thermal boundary layer.

The cause of the enhancement mechanism associated with a dilute solution of hexane in R123 is different from that observed for surfactants in aqueous solutions. Surfactants in water lower the surface-tension of the liquid–vapor interface. In contrast, the hexane lowers the surface-tension of the liquid–solid interface. There are two reasons why hexane cannot lower

the liquid–vapor interface surface-tension of R123. First, the surface-tension of hexane (0.02 N/m) is larger than that of R123 (0.018 N/m), so the hexane is repelled from the liquid–vapor interface. Second, a surfactant must have a polar end (a lyophilic group) that is attracted to the polar solvent to establish a stable liquid–vapor interface structure. Hexane has a zero dipole moment. Therefore, hexane does not have the characteristic molecular structure of a surfactant.

CONCLUSIONS

The pool boiling performance of R123 on a GEWA-T^{TM} surface was enhanced as much as $(47 \pm 7)\%$ by adding 1% mass hexane. The maximum percent heat flux enhancement for R123/hexane (99/2) mixture was $(29 \pm 7)\%$. Observations from high-speed 16 mm films of the boiling revealed that the addition of hexane to pure R123 causes a simultaneous reduction in the bubble diameter and an increase in the site density. The pool boiling enhancement mechanism is presumably due to an accumulation of hexane at the boiling surface in the channels. Apparently, the excess layer reduces the surface-energy between the liquid and the heat transfer surface causing the production of small diameter bubbles. Smaller bubbles will induce higher site densities than larger bubbles. The site density is increased enough to more than compensate for the loss in bubble size and result in a net heat transfer enhancement.

Acknowledgements

This work was jointly funded by NIST, Dupont, and the U.S. Department of Energy (project no. DE-01-95CE23808.000 modification #A004) under Project Managers Glenn Shealy and Bill Noel, respectively. Thanks goes to the following NIST personnel for their constructive criticism of the first draft of the manuscript: Dr. D. A. Didion, Dr. M. O. McLinden, Mr. P. I. Rothfleisch, and Mrs. J. Land. The author would also like to express appreciation to E. Bellinger and A. Dashottar for data collection. Furthermore, the author extends appreciation to Dr. E. Lagergren for consultations on the uncertainty analysis.

NOMENCLATURE

English Symbols

A	coefficients for Laplace equation
A_s	actual surface area (m)
C	molar concentration of the solute
D_b	departure bubble diameter (m)
E_{Tw}	expanded uncertainty in the wall temperature (K)
$E_{q''}$	relative expanded uncertainty (%) in heat flux measurement
e	height of fin from tip to root (m)
k	thermal conductivity (W/m·K)
L_y	length of test surface (m)
p	exterior perimeter of test surface (m)
q''	average wall heat flux (W/m^2)
R	universal gas constant (8.314 J/K·mol)
Ra_L	Rayleigh number based on A_s/p
r_c	radius of cavity mouth (m)
S_f	spacing or gap between fin-tips (m)
s	estimate of standard deviation
T	temperature (K)
T_w	temperature of surface at root of fin (K)
U	expanded uncertainty
u_i	standard uncertainty
x	test surface coordinate, (Fig. 2) (m)
y	test surface coordinate, (Fig. 2) (m)

Greek Symbols

β	contact angle (rad)
Γ	surface excess concentration of solute
δ_t	thermal boundary layer thickness (m)
ΔT	wall superheat: $T_w - T_s$, (K)
σ	surface-tension (kg/s^2)

Subscripts

1%	R123/hexane (99/1)
2%	R123/hexane (98/2)
i	interface
l	liquid
m	mixture
p	pure R123
s	saturated state, solid surface
v	vapor

Superscript

-	average

References

Adamson, A. W. (1967) Physical Chemistry of Surfaces, Interscience Publ., New York, 2nd ed., p. 353.

Ayub, Z. H. and Bergles, A. E. (1987) "Pool Boiling from GEWA Surfaces in Water and R-113" *Wärme- und Stoffübertragung*, **21**, 209–219.

Carey, V. P. (1992) Liquid-Vapor Phase-Change Phenomena, Hemisphere, Washington.

Cornwell, K. and Einarsson, J. G. (1989) "The Influence of Fluid Flow on Nucleate Boiling from a Tube", Eurotherm Seminar No. 8, Advances in Pool Boiling Heat Transfer, Paderborn, FRG, May 11–12, pp. 28–41.

Eckert, E. R. G. and Goldstein, R. J. (1976) Measurements in Heat Transfer, Hemisphere, Washington, 2nd ed., pp. 9–11.

Glamm, P. (1995) Private communications, The Trane Company, La Crosse, Wisconsin.

Hsu, Y. Y. (1962) "On the Size Range of Active Nucleation Cavities on a Heating Surface", *J. Heat Transfer*, **84**, 207–216.

Incropera, F. P. and DeWitt, D. P. (1985) Fundamentals of Heat and Mass Transfer, 2nd ed., John Wiley & Sons, New York, p. 439.

Jontz, P. D. and Myers, J. E. (1960) "The Effect of Dynamic Surface Tension on Nucleate Boiling Coefficients", *AICHE Journal*, **6**(1), pp. 34–38.

Kedzierski, M. A. (1993) "Simultaneous Visual and Calorimetric Measurements of R11, R123, and R123/Alkylbenzene Nucleate Flow Boiling", Heat Transfer with Alternative Refrigerants, ASME HTD Vol. 243, H. J. Sauer, Jr. and T. H. Kuehn, Eds., ASME, New York, pp. 27–33.

Kedzierski, M. A. (1995) "Calorimetric and Visual Measurements of R123 Pool Boiling on Four Enhanced Surfaces", NISTIR 5732, U.S. Department of Commerce, Washington.

Kedzierski, M. A. (1996) "Enhancement of R123 Pool Boiling by the Addition of *N*-Hexane", NISTIR 5780, U.S. Department of Commerce, Washington.

Kedzierski, M. A. and Kaul, M. P. (1993) "Horizontal Nucleate Flow Boiling Heat-transfer-coefficient Measurements and Visual Observations for R12, R123, and R123/Ester Lubricant Mixtures", *6th Int. Symp. on Transport Phenomena in Thermal Engineering*, Seoul, Korea, **I**, 111–116.

Kedzierski, M. A. and Worthington, J. L. III (1993) "Design and Machining of Copper Specimens with Micro Holes for Accurate Heat Transfer Measurements", *Experimental Heat Transfer*, **6**, 329–344.

Morrison, G. and McLinden, M. O. (1985) "Application of a Hard Sphere Equation of State to Refrigerants and Refrigerant Mixtures", NBS Technical Note 1226, National Bureau of Standards, Gaithersburg, MD.

Morrison, G. and Ward, D. K. (1991) "Thermodynamic Properties of Two Alternative Refrigerants: 1,1-Dichloro-2,2,2-Trifluoroethane (R123) and 1,1,1,2-Tetrafluoroethane (R134a)", *Fluid Phase Equilibria*, **62**, 65–86.

Rosen, M. J. (1978) Surfactants and Interfacial Phenomena, John Wiley & Sons, New York, p.57.

Shah, B. H. and Darby, R. (1973) "The Effect of Surfactant on Evaporative Heat Transfer in Vertical Film Flow", *Int. J. Heat Mass Transfer*, **16**, 1889–1903.

Shealy, G. S. (1993) Private communications, Du Pont Chemicals, Wilmington, Deleware.

Shock, R. A. W. (1982) "Boiling in Multicomponent Fluids", Multiphase Science and Technology, Hemisphere Publishing Corp., **1**, 281–386.

Siu, M. C. I., Carroll, W. L. and Watson, T. W. (1976) "Thermal Conductivity and Electrical Resistivity of Six Copper-Base Alloys", NBSIR 76-1003, U.S. Department of Commerce, Washington.

Thome, J. R. (1990) Enhanced Boiling Heat Transfer, Hemisphere Publishing Corp., New York, Chap. 9.

Tzan, Y. L. and Yang, Y. M. (1990) "Experimental Study of Surfactant Effects on Pool Boiling Heat Transfer", *J. Heat Transfer*, **112**, 207–212.

Webb, R.L. and Pais, C. (1992) "Nucleate Pool Boiling Data for Five Refrigerants on Plain, Integral-fin and Enhanced Tube Geometries", *Int. J. Heat Mass Transfer*, **35**(8), pp. 1893–1904.

Westwater, J. W. (1956) "Boiling of Liquids", Advances in Chemical Engineering, Vol. 1, T. B. Drew and J. W. Hoopes, Jr., Eds., Academic Press, New York.

Wu, W., Yang, Y. and Maa, J. (1995) "Enhancement of Nucleate Boiling Heat Transfer and Depression of Surface Tension by Surfactant Additives", *J. Heat Transfer*, **117**, 526–529.